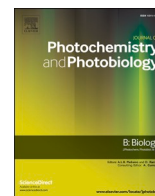




Contents lists available at ScienceDirect

Journal of Photochemistry & Photobiology, B: Biology

journal homepage: www.elsevier.com/locate/jphotobiol

Fluorescence lifetime imaging and phasor analysis of intracellular porphyrinic photosensitizers applied with different polymeric formulations

Florentin S. Spadin^a, Lea P. Gergely^b, Tobias Kämpfer^b, Martin Frenz^{a,*}, Martina Vermathen^{b,*}

^a Institute of Applied Physics, University of Bern, Sidlerstrasse 5, 3012 Bern, Switzerland

^b Department of Chemistry, Biochemistry and Pharmaceutical Sciences, Freiestrasse 3, 3012 Bern, Switzerland

ARTICLE INFO

Keywords:

Fluorescence lifetime imaging
Phasor analysis
Photosensitizer
Drug delivery
PVP
Block copolymer micelles
Cremophor

ABSTRACT

The fluorescence lifetime of a porphyrinic photosensitizer (PS) is an important parameter to assess the aggregation state of the PS even in complex biological environments. Aggregation-induced quenching of the PS can significantly reduce the yield of singlet oxygen generation and thus its efficiency as a medical drug in photodynamic therapy (PDT) of diseased tissues. Hydrophobicity and the tendency to form aggregates pose challenges on the development of efficient PSs and often require carrier systems. A systematic study was performed to probe the impact of PS structure and encapsulation into polymeric carriers on the fluorescence lifetime in solution and in the intracellular environment. Five different porphyrinic PSs including chlorin e6 (Ce6) derivatives and tetrakis(*m*-hydroxyphenyl)-porphyrin and -chlorin were studied in free form and combined with polyvinylpyrrolidone (PVP) or micelles composed of triblock-copolymers or Cremophor. Following incubation of HeLa cells with these systems, fluorescence lifetime imaging combined with phasor analysis and image segmentation was applied to study the lifetime distribution in the intracellular surrounding. The data suggest that for free PSs, the structure-dependent cell uptake pathways determine their state and emission lifetimes. PS localization in the plasma membrane yielded mostly monomers with long fluorescence lifetimes whereas the endocytic pathway with subsequent lysosomal deposition adds a short-lived component for hydrophilic anionic PSs. Prolonged incubation times led to increasing contributions from short-lived components that derive from aggregates mainly localized in the cytoplasm. Encapsulation of PSs into polymeric carriers led to monomerization and mostly fluorescence emission decays with long fluorescence lifetimes in solution. However, the efficiency depended on the binding strength that was most pronounced for PVP. In the cellular environment, PVP was able to maintain monomeric long-lived species over prolonged incubation times. This was most pronounced for Ce6 derivatives with a log P value around 4.5. Micellar encapsulation led to faster release of the PSs resulting in multiple components with long and short fluorescence lifetimes. The hydrophilic hardly aggregating PS exhibited a mostly stable invariant lifetime distribution over time with both carriers. The presented data are expected to contribute to optimized PDT treatment protocols and improved PS-carrier design for preventing intracellular fluorescence quenching. In conclusion, amphiphilic and concurrent hydrophobic PSs with high membrane affinity as well as strong binding to the carrier have best prospects to maintain their photophysical properties in vivo and serve thus as efficient photodynamic diagnosis and PDT drugs.

1. Introduction

Porphyrinic photosensitizers (PSs) are used in photodynamic

diagnosis (PDD) and therapy (PDT) of diseased tissue and in theranostic approaches combining PDD and PDT in one treatment [1,2]. The PSs are distinguished by their photophysical properties including light

Abbreviations: Ce4, chlorin e4; Ce6, Chlorin e6; CeDME, Ce6-dimethylester; DMSO, Dimethyl sulfoxide; ER, Endoplasmic reticulum; FBS, Fetal bovine serum; FLIM, Fluorescence lifetime imaging microscopy; HLB, Hydrophilic-lipophilic balance; KP, Kolliphor P188; MEM, Minimum essential medium; m-THPP, Tetrakis(*m*-hydroxyphenyl)chlorin; m-THPP, Tetrakis(*m*-hydroxyphenyl)porphyrin; PBS, Phosphate buffered saline; PDD, Photodynamic diagnosis; PDT, Photodynamic therapy; PEG, Polyethylene-glycol; PFA, Paraformaldehyde; PPG, Polypropylene-glycol; PS, Photosensitizer; PVP, Polyvinylpyrrolidone; RH, Kolliphor RH 40; SerCe, Ce6-serine amide..

* Corresponding authors.

E-mail addresses: martin.frenz@unibe.ch (M. Frenz), martina.vermathen@unibe.ch (M. Vermathen).

<https://doi.org/10.1016/j.jphotobiol.2024.112904>

Received 9 December 2023; Received in revised form 6 March 2024; Accepted 1 April 2024

Available online 3 April 2024

1011-1344/© 2024 The Authors. Published by Elsevier B.V. This is an open access article under the CC BY license (<http://creativecommons.org/licenses/by/4.0/>).

absorption in the therapeutic window of 650–850 nm where tissue penetration of light is optimal [3]. They exhibit fluorescence emission from their excited singlet states with structure-dependent fluorescence quantum yields typically lying in the range of 10% for free-base porphyrins [4,5] but also less or about two- to four times higher [5,6]. The formation of highly reactive singlet oxygen through energy transfer from the PSs' excited triplet states to molecular oxygen is mostly responsible for controlled tissue damage in PDT [1,7]. In addition, porphyrinic PSs normally show low dark toxicity and accumulate in proliferating tissues [8]. The development of efficient porphyrinic PSs faces challenges due to their often low water solubility and pronounced tendency to form aggregates via stacking of the planar macrocyclic ring systems leading to fluorescence quenching and consequential loss of their photodynamic activity [9,10]. This can be overcome by using suitable drug delivery systems, mostly nanosized particles of organic or inorganic materials. Therefore, today, PSs are often applied in combination with specific supramolecular, nanosized carriers [11,12]. Carriers enhance the solubility of the drug. They protect the drug during transport through the blood stream by preventing its premature clearance, reduce drug toxicity and thus side effects. Carriers possibly increase tumor accumulation via the enhanced permeability and retention effect and can provide a platform for targeting using specific surface ligands or for combining different drugs by co-encapsulation.

Consequently, studying the relevant photophysical properties of a given PS are ideally performed in the biological environment under consideration of its formulation. Structure, form, and size of carrier-nanoparticles affect cell uptake mechanisms and intracellular fate of the encapsulated drug molecules [13–15]. The intracellular PS localization and interaction with cell components, i.e., the immediate molecular surrounding of the PS inside the cell, finally govern its photodynamic efficiency and type of cell death pathways [16,17]. Numerous studies have addressed the intracellular distribution of porphyrinic PSs by fluorescence microscopy taking advantage of the inherent fluorescence of the porphyrinic compound and applying co-staining with organelle specific fluorescent probes. These studies revealed that subcellular localization mainly takes place in lysosomes, plasma membranes, mitochondria, cytosol, or endoplasmic reticulum (ER) [16,18], but rarely in the nucleus. While the fluorescence intensity thus provides valuable information about the spatial distribution and the overall amount of the intracellular porphyrinic PS, it remains unclear, to what extent aggregated or bound species are present. Moreover, the PS fluorescence may overlap with autofluorescence deriving from cell components [19–21].

Studying the temporal evolution, i.e., the fluorescence decay dynamics, adds with the time-component further information to the fluorescence maps. This enhances the analytical selectivity for the fluorophore of interest, since the porphyrinic PSs typically have different fluorescence lifetimes compared to those of cell components. Moreover, the fluorescence decay dynamics are sensitive measures for PS aggregation and intermolecular interactions and are able to discriminate between different species of the same compound [22]. Therefore, fluorescence lifetime imaging microscopy (FLIM) is a powerful tool that allows monitoring spatially resolved fluorescence lifetimes of fluorophores in biological material like tissue or cells [10,21–24].

In the past, several studies have applied FLIM to address the fluorescence decay dynamics of porphyrinic PSs in various biological environments. They included the intracellular distribution of porphyrins [25–28], chlorins [28–31], phthalocyanines [32–34], bacteriochlorin distribution in mice [35], and PS distribution in tissue [36] and bacterial biofilms [37]. FLIM indicated different environments of porphyrins in normal and cancer cells [38]. Recently, it has been shown that the fluorescence lifetime of intracellular Ce6 derivatives is pH dependent and that this in turn contributed to localization-dependent emission decays of the PS, mainly in cytoplasm and lysosomes [31]. Notably, the intracellular aggregation behavior of porphyrinic PSs has been

addressed by FLIM [28–30]. It has been shown that the fluorescence lifetime of intracellular PSs decreases over time possibly due to aggregation as was observed for tetrakis(*m*-hydroxyphenyl)chlorin (*m*-THPC) [28,29] and for protoporphyrin IX [26,28].

However, the impact of drug delivery systems on the intracellular fluorescence lifetimes of porphyrinic PSs has been rarely addressed. The aim of the current study was therefore, to determine how polymeric carrier systems could affect the time-resolved fluorescence emission dynamics of different porphyrinic PSs in the cellular environment. By incubating cultured cancer cells for different periods with pure or carrier-encapsulated PSs, it was investigated if the previously described intracellular PS aggregation could be prevented or reduced by the carrier. For this, a systematic study was performed using a series of structurally related Ce6 derivatives as well as tetrakis(*m*-hydroxyphenyl)porphyrin (*m*-THPP) and *m*-THPC (temoporphin, active substance in the medicinal form Foscan®), the latter being an approved PDT drug [39] (Fig. 1). Structure selection was guided by the aim to cover PSs with a range of log*P* values and thus with differently pronounced tendencies to form aggregates in aqueous solutions. The PSs shown in Fig. 1 were combined with three different types of carriers for physical encapsulation. These included polyvinylpyrrolidone (PVP) that forms a molecular network (Fig. 2A) and is an approved, commonly applied and versatile carrier system for a wide range of drugs [40,41]. In addition, the micelle forming triblock-copolymer Kolliphor P188 (KP, Fig. 2B) and the Polyethylene-glycol-(PEG) ester of hydrogenated castor oil Kolliphor RH 40 (RH, Cremophor, Fig. 2C) were used. Initially, the fluorescence lifetime of the pure PS and PS-carriers was determined in solution. Subsequently, FLIM was applied to HeLa-cells following treatment with the various PS formulations. The resulting fluorescence lifetime images were evaluated based on single pixel fitting, image segmentation, and phasor analysis. The phasor approach is a very powerful method allowing for the visualization of populations with similar decay dynamics as clusters in the phasor space [42]. It has already been applied to show the presence of different porphyrin species [31,37] and to distinguish porphyrin clusters from intrinsic fluorophores in cells and tissues like skin [36].

2. Materials and Methods

2.1. Materials

2.1.1. Chemicals

The PSs Ce6, Ce6-serine amide (SerCe), chlorin e4 (Ce4), and Ce6-dimethyl ester (CeDME) were obtained from Frontier Scientific (Logan, Utah). 5,10,15,20-Tetrakis(*m*-hydroxyphenyl)porphyrin (*m*-THPP) [43] and 5,10,15,20-Tetrakis(*m*-hydroxyphenyl)chlorin (*m*-THPC) were kindly provided by the biolitec research GmbH, Jena, Germany. PVP (average MW = 10 kDa), the PEG-polypropylene glycol (PPG)-PEG triblock-copolymer Kolliphor® P188 (KP, average MW = 8.4 kDa), and the PEG-ester of hydrogenated castor oil Kolliphor® RH 40 (RH, average MW = 2.5 kDa) were purchased from Sigma-Aldrich (Buchs, Switzerland). Phosphate buffered saline (PBS, 50 mM, pH = 7.3) was prepared by mixing aliquots of 50 mM solutions of KH₂PO₄ and Na₂HPO₄ (provided by Sigma-Aldrich) in H₂O containing 0.9% NaCl.

2.1.2. Cell Culture

The human epithelioid cervix carcinoma HeLa Cell Line originating from the European collection of authenticated cell cultures (ECACC) was purchased from Merck and was tested for absence of mycoplasma contamination upon arrival. Cells were cultured in minimum essential medium (MEM, Gibco) supplemented with 10% fetal bovine serum (FBS), 1% non-essential amino acids, 1% Penicillin-streptomycin-glutamine, 0.5% Chlorotetracycline, 0.5% sodium-pyruvate and 0.1% uridine. The cells were cultivated in 75 cm² flasks at 37 °C with 5% CO₂ and passaged twice a week by washing twice with 5 mL PBS, trypsinated for 5 min with 2 mL trypsin-EDTA (0.05%) and deactivated with 2 mL

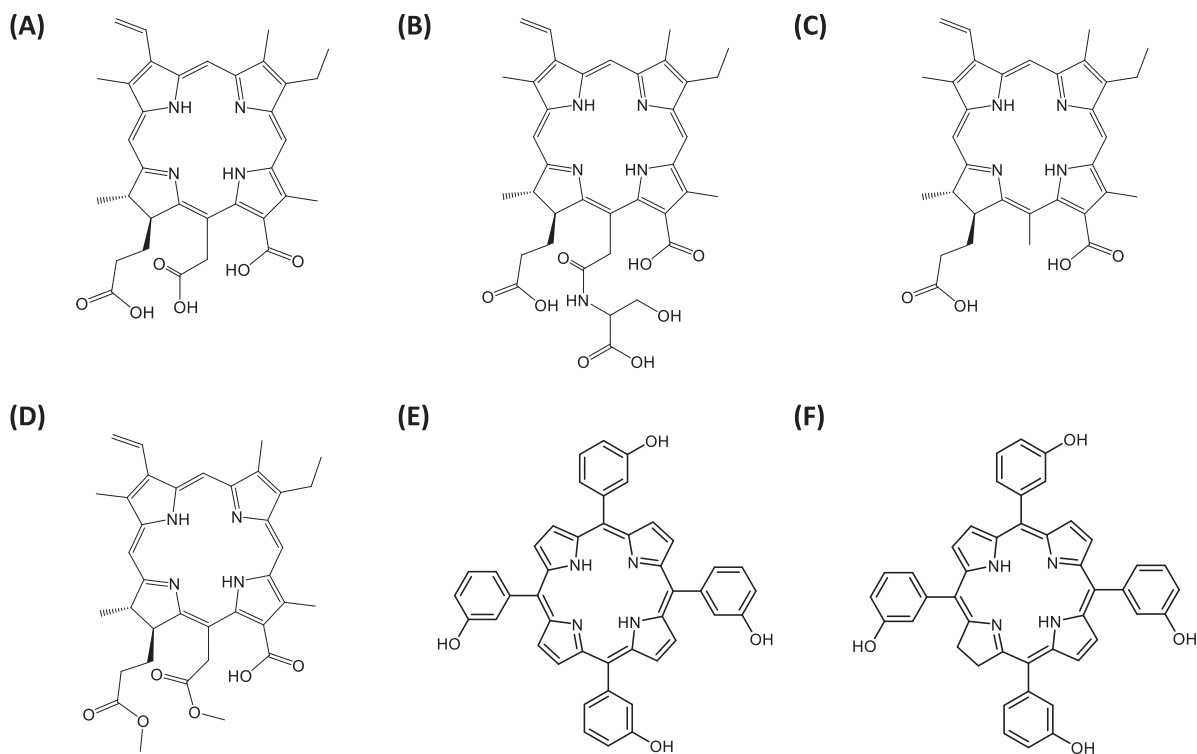


Fig. 1. Structures of the photosensitizers (A) Chlorin e6 (Ce6); (B) Chlorin e6 serine amide (SerCe); (C) Chlorin e4 (Ce4); (D) Chlorin e6 dimethyl ester (CeDME); (E) 5,10,15,20-Tetrakis(*m*-hydroxyphenyl)porphyrin (m-THPP); and (F) 5,10,15,20-Tetrakis(*m*-hydroxyphenyl)chlorin (m-THPC).

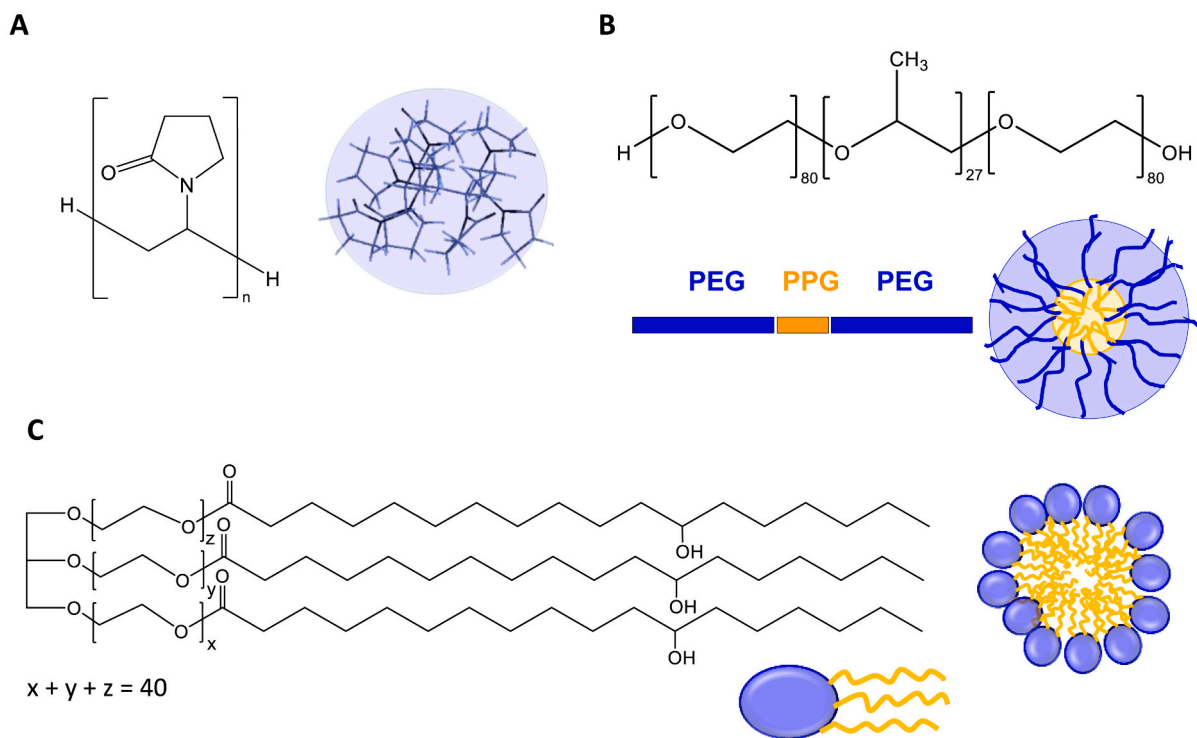


Fig. 2. Structures of the polymeric carrier units and sketch of the carrier particles (A) Polyvinylpyrrolidone (PVP) and PVP-network; (B) Polyethylene-block-polypropylene-polyethylene-glycol Kolliphor P188 (KP) and KP-micelles; (C) Polyethylene-glycol-ester of hydrogenated castor oil Kolliphor RH 40 (RH, Cremophor) and RH-micelle.

MEM. Cells were stored in freezing medium containing 10% dimethyl sulfoxide (DMSO), 10% FBS and 80% MEM. Paraformaldehyde (PFA, 16%, Electron Microscopy Sciences) was used for cell fixation.

2.2. Sample Preparation

2.2.1. Solutions for Fluorescence Lifetime Measurements

For each of the porphyrinic compounds Ce6, SerCe, Ce4, m-THPP, and m-THPC, a solution in ethanol was prepared at concentrations of 1 μM and 100 μM . In addition, aqueous solutions of each compound were prepared at concentrations of 1 μM , 10 μM , and 100 μM without carriers, as well as encapsulated in KP or PVP. For this, 1 mM stock solutions of the PSs in DMSO were diluted with water or a solution of the carrier in water to obtain the desired PS concentrations (final DMSO conc. 2%). The concentration of KP was kept constant at 3 mM, which is well above the critical micelle concentration (cmc) of approximately 0.45 mM [44]. For PVP, the molar ratio of PVP: PS was 10: 3. The measurement of the first time point ($t = 0$ h) was performed immediately after dilution. Follow-up measurements of each solution were performed after 1 day and after 4 days. During this time, the solutions were left standing in the dark at room temperature.

2.2.2. HeLa Cells Incubated with Varying Formulations of Porphyrinic PSs

The following incubation solutions were prepared using a stock solution of 1 mM PS in DMSO: (i) 5 μM PS in PBS; (ii) 5 μM PS / 16.7 μM PVP; (iii) 5 μM PS / 3 mM KP or 3 mM RH. Cells were counted and seeded on coverslips into 12 well plates in 1 mL MEM to reach a density of 360 cells/ mm^2 after incubation time (HeLa doubling time is 35 h). Cells were incubated either with 5 μM pure PS solutions or with 5 μM PS / carrier solution and kept in dark. Exposure to the PS solutions was 3 h, 12 h, and 24 h. Afterwards cells were collected and washed with PBS, fixed with 150 μL of 4% PFA for 15 min and washed twice with PBS. Then the coverslips were flipped onto a microscopy slide with PBS as mounting medium and sealed with nail polish. The samples were kept in the fridge until measurements were recorded. Efficient uptake of Ce6 derivatives either alone or associated with PVP or KP by HeLa cells has been shown in previous studies using flow cytometry [6,15].

According to the above sample preparations, all PS concentrations mentioned in this study (1/10/100 μM for solutions and 5 μM for cells) refer to the PS concentration that was initially added to the solution or loading medium. Potential non-encapsulated PSs were not removed, because all fluorescence lifetime data obtained with carriers were compared to the corresponding carrier-free samples as reference. Moreover, this approach allowed to monitor – where applicable – potential further disaggregation over time in the presence of carriers or upon cell entry.

2.3. Fluorescence Lifetime Measurements

2.3.1. Instrumentation

Fluorescence lifetime measurements were conducted in time-correlated single photon counting (TCSPC) mode using a Zeiss LSM 10 confocal laser-scanning microscope adapted for fluorescence lifetime imaging using a FLIM upgrade kit (Becker & Hickl PZ-FLIM-110). A Zeiss Achromplan 40 \times objective with a numerical aperture of 0.75 was used, resulting in a theoretical optical section thickness of at minimum 3.1 μm .

Fluorescence excitation was conducted using a pulsed diode laser (PicoQuant LDH-C 400) with a wavelength of 405 nm and a pulse length of 130 ps. While for in vivo PDT longer excitation wavelengths in the optimal therapeutic window are advantageous, the excitation wavelength of 405 nm used here has often been applied in fluorescence lifetime studies on porphyrinic compounds in the literature [22] and is expected not to affect the fluorescence lifetime according to previous reports [45]. Emission was measured from 590 nm to 720 nm. Measurements were conducted at a pulse repetition rate of 20 MHz, yielding an average photon counting rate of 10^5 s^{-1} .

The setup further includes a piezo scanning stage (Mad City Labs NanoStage) with a maximum scan area of $200 \times 200 \mu\text{m}^2$ and a bright field illumination system used for FOV acquisition. The detector used was a Becker & Hickl HPM-100-40 hybrid PMT, together with a Becker & Hickl SPC-160 digitizer card. The entire setup was controlled through the Becker & Hickl SPCM64 software.

2.3.2. Data Analysis

Measurements were analyzed using SPCImageNG software (Becker & Hickl). Fluorescence decay curves were fitted using eq. (1)

$$F(t) = \sum_{i=1}^n A_i \cdot \exp\left(-\frac{t}{\tau_i}\right) \quad (1)$$

where τ_i represents the individual fluorescence lifetimes and A_i the molar fraction of i components. For model-based evaluation, a multi-exponential model was used with lifetimes τ_i constrained to the interval [0, 99] ns. The Instrument Response Function (IRF) was estimated from the decay curve by differentiation of the rising edge and therefore did not need to be measured explicitly.

Phasor data was calculated in SPCImageNG and subsequently exported for further processing in Python using NumPy and scikit-image modules. Cell membrane masking was accomplished manually in SPCImageNG.

3. Results and Discussion

3.1. Fluorescence Lifetime of PSs in Solution

Porphyrinic compounds have a high tendency to form aggregates in water via stacking of their planar π -conjugated ring systems. Besides π - π -interactions, hydrophobic van der Waals as well as electrostatic interactions and hydrogen bonding can contribute to aggregate formation and stabilization. The extent of aggregation depends on factors like concentration, temperature, solvent, hydrophobicity, and peripheral substitution pattern [46–48]. Depending on the arrangement of the self-assembled macrocycles, either H-aggregates with parallel stacked face-to-face units or J-aggregates with slipped head-to-tail units are formed [49]. Both, aggregate structure, and size have a pronounced impact on the photophysical properties of the PS [49,50]. While H-aggregates are—with a few exceptions—non-emissive, J-aggregates exhibit fluorescence [51]. However, their fluorescence lifetimes are in general strongly reduced upon dimer or higher aggregate formation where non-radiative processes prevail leading to fluorescence quenching [19,50].

In the present study, the fluorescence lifetimes of five PSs, namely SerCe, Ce6, Ce4, m-THPP, and m-THPC (Fig. 1), were initially studied in aqueous solution without carriers as well as encapsulated either in PVP or KP (Fig. 2), before cell experiments were performed. To probe the impact of potential aggregation onto the lifetimes, different PS concentrations were applied (1 μM , 10 μM , and 100 μM) and the solutions were left standing at room temperature and measured at three time points (0, 1 d, and 4 d). The resulting τ -values for the different conditions are displayed as bar plots in Fig. 3. While for the Ce6 derivatives (SerCe, Ce6, Ce4) uniform decay curves were obtained not indicating pronounced fluorescence quenching (Figs. S1-S3), the decay curves for m-THPP and m-THPC clearly appeared more heterogeneous indicating the presence of quenched short-lived components (Figs. S4 and S5). The main reason for this is most likely the higher tendency of m-THPP and m-THPC to form aggregates in aqueous solutions as will be outlined in more detail below (see 3.1.1). For comparison, the pure PSs were also measured in ethanol solution (Table 1) where they mostly exist as monomers.

3.1.1. Fluorescence Lifetime of PSs in Solution Without Carriers

3.1.1.1. Ce6 Derivatives. In aqueous solution, SerCe, Ce6, and Ce4 had

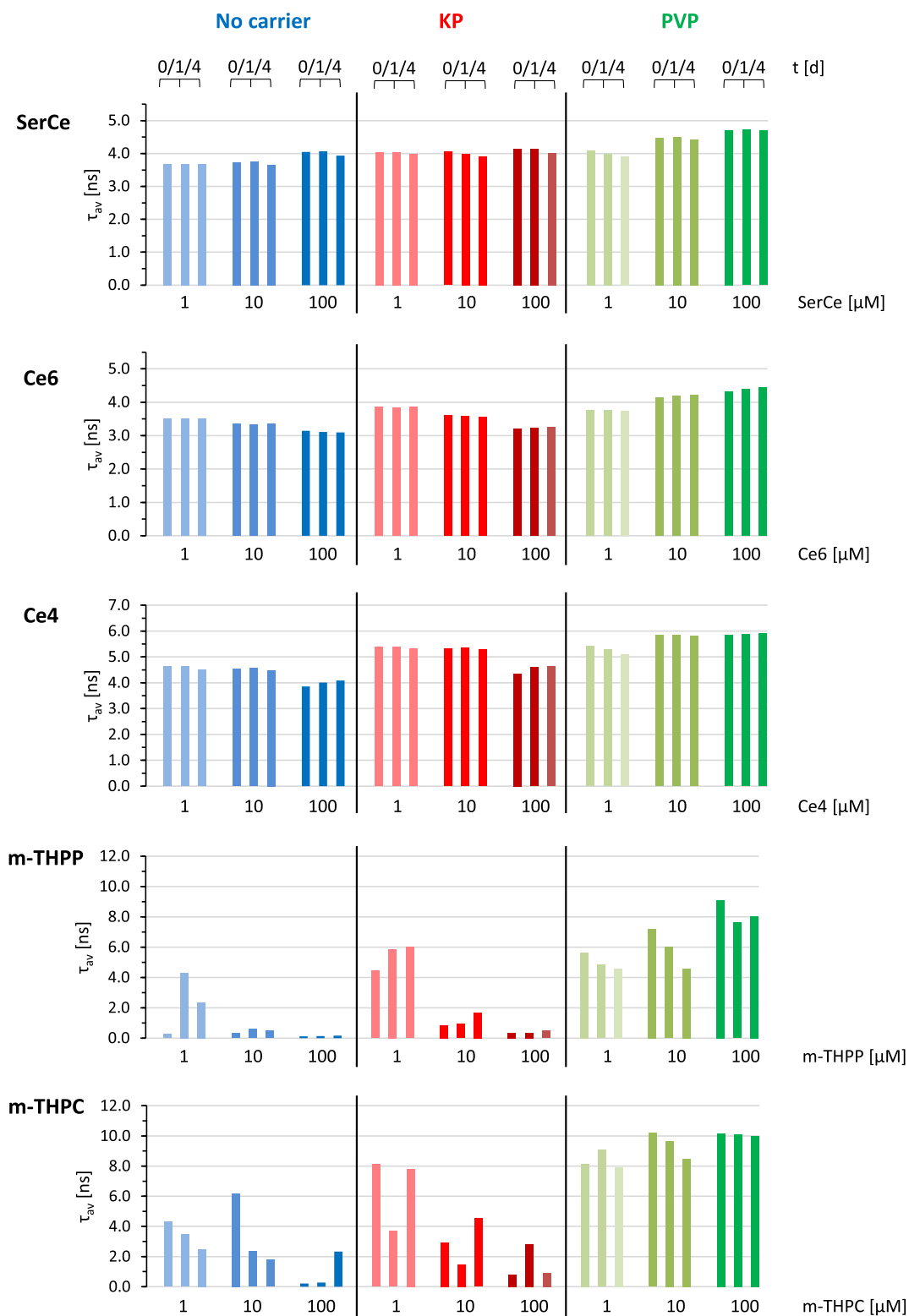


Fig. 3. Fluorescence lifetimes of the PSs SerCe, Ce6, Ce4, m-THPP and m-THPC in water (2% DMSO) solutions in the absence (blue) and presence of the carriers KP (red) and PVP (green). PS concentrations were 1 μM , 10 μM , and 100 μM . Each solution was measured immediately after preparation ($t = 0$) and subsequently after 1 day and 4 days. The fluorescence decay curves were fitted with a multi-exponential function (displayed are the weighted average lifetimes τ_{av}). Decay curves, fit-curves and χ^2 -values are given in the supporting material (Figs. S1-S5). (For interpretation of the references to colour in this figure legend, the reader is referred to the web version of this article.)

Table 1

Calculated log*P* values of PSs and measured average fluorescence lifetimes τ_i in ethanol solution from exponentially fitted decay curves (A_i : fraction of each component).

PS	Log <i>P</i> ^a	Conc. [μ M]	τ_1 [ns] (A_1)	τ_2 [ns] (A_2)	χ^2_r
SerCe	2.46	1	4.54 (1)	-	1.27
		100	n.d. ^b	-	-
Ce6	3.39	1	4.65 (1)	-	1.18
		100	5.19 (0.55)	3.95 (0.45)	1.06
Ce4	4.64	1	5.36 (1)	-	1.15
		100	5.45 (1)	-	1.15
CeDME	4.68		5.20 ^c (1)	-	-
m-THPC	6.80	1	8.80 (1)	-	1.18
		100	8.85 (1)	-	1.29
m-THPP	6.84	1	9.72 (0.30)	0.30 (0.70)	1.34
		100	11.54 (0.35)	9.26 (0.65)	1.06

^a calculated based on smiles using the free software «ALOGPS2.1» [52]

^b not determined

^c Value reported for CeDME in acetone [53].

similar emission lifetimes between 3 ns and 5 ns with only small changes over time and over the concentration range between 1 μ M and 100 μ M. This indicates that the Ce6 derivatives mainly exist as monomers in water under the applied conditions, since the fluorescence lifetime is a concentration independent parameter. However, the log*P* value and thus the hydrophobicity increases from SerCe to Ce4 by two units (Table 1). Our previous studies have shown that Ce4 indeed has a higher tendency to self-assemble with an onset of aggregation in PBS at a concentration of 2 μ M [6] whereas dimerization was observed for SerCe around 20 μ M [44]. Usage of water (2% DMSO) instead of PBS may account for a stabilization of the monomeric state in the present set-up since high salt concentrations were shown to favor aggregate formation of water soluble porphyrins [54]. Nevertheless, decreased τ -values observed for Ce6 and Ce4 at a concentration of 100 μ M compared to 1 μ M suggest contributions from faster decaying dimeric or oligomeric species to the overall emission curves. The fluorescence lifetimes of the Ce6 derivatives measured in ethanol (4.5–5.5 ns, Table 1) agreed well with literature values [22] and were longer than the ones determined in aqueous solution. This difference can be explained by the solvent effect that leads to faster decays with increasing solvent polarity, since fluorophores exhibit larger dipole moments in the excited states [22,55].

3.1.1.2. m-THPP and m-THPC. For the two meso-substituted PSs m-THPP and m-THPC, a strong decrease of the fluorescence lifetime in water solution was observed even at the lowest concentration of 1 μ M with τ -values between 0.3 ns and 4.5 ns (Fig. 3) compared to τ -values of around 9 ns in ethanol solutions (Table 1). This indicates pronounced aggregate formation in aqueous solution that goes along with larger log*P* values for these compounds compared to the Ce6 derivatives (Table 1). For m-THPP, the emission decays were also bi-exponential in ethanol. The second rather long-lived species for m-THPP at 100 μ M (9.26 ns) is most likely due to J-type dimer formation and the same may hold for Ce6 (5.19 ns and 3.95 ns, Table 1). The aggregation behavior of m-THPP and m-THPC is well documented in the literature where the formation of J-type (also H-type in case of m-THPP) aggregates in water and water-alcohol mixtures was proposed [56,57]. For m-THPC in water, there was also a drop in τ -values over time (0, 1d, 4d) at 1 μ M and 10 μ M (Fig. 3). This is in agreement with the previously reported time-dependent intracellular lifetime decrease of m-THPC from 8 ns to 5 ns over a period of 21 h, which was mainly attributed to increased aggregation besides potential contributions from self-quenching [29]. Such time evolution of self-assembled supramolecular structures is often encountered with porphyrinic compounds in aqueous media and constitutes a rather unwanted feature in PDT whereas controlled growth can be of advantage in other applications like the development of functional nanomaterials [58,59].

3.1.2. Fluorescence Lifetime of PSs in Solution in the Presence of Carriers

3.1.2.1. Ce6 Derivatives. Encapsulation of the Ce6 derivatives SerCe, Ce6, and Ce4, into KP micelles and PVP yielded prolonged fluorescence lifetimes compared to the pure, carrier-free compounds in aqueous solution (Fig. 3) and similar or even longer compared to ethanol solutions (Table 1). The increase was most pronounced for PVP each at the highest chlorin concentration of 100 μ M and the τ -values were constant over time at any of the applied concentrations. Previously, we have shown that amphiphilic Ce6 derivatives are well encapsulated as monomers in PVP [6,44,60]. Likewise, Ce6, SerCe, and Ce4 exist as monomers in KP-micelles [6,44,61]. The overall longer lifetimes in both carriers can be mainly explained by the above-mentioned solvent effect [22,55]. Upon encapsulation, the chlorin molecules change from the aqueous bulk solution into a hydrophobic microenvironment formed by the micellar core and by the cavities in the PVP network. Additional contributions may derive from carrier-mediated dissolution of small fractions of aggregates existing in water. Similar observations of increased fluorescence lifetimes have been reported for porphyrinic PSs embedded into liposomes [62], surfactant micelles [63,64], or chitosan/PEG films [65], in which the hydrophobic PS-polymer/lipid interactions were the driving force for disaggregation and localization in the carrier.

In KP micelles, Ce4 and Ce6 exhibited shorter τ -values at the highest concentration of 100 μ M compared to 1 and 10 μ M and compared to PVP (Fig. 3). Micellar systems are in general characterized by internal mobility and flexibility of their single polymer chains [6,63,66] or with subdomains of different flexibilities [67], respectively. This allows for encapsulated drugs to undergo exchange processes between the micellar and the surrounding polar aqueous environment. Thus, the reduced τ -values at 100 μ M are most likely due to a small fraction of aggregates as short-lived components in water coexisting with the main long-lived components in the micellar compartment. According to our previous results, drug binding to PVP is clearly stronger than to micelles thus repelling exchange with the surrounding aqueous medium [6,34,44]. Therefore, the consistently long lifetimes measured in PVP can be attributed to PSs (almost) exclusively residing in the PVP network. For micelles, the equilibrium shifts from the aqueous towards the micelle compartment with increasing hydrophobicity of the encapsulated PS following the order Ce4 > Ce6 > SerCe. However, since SerCe does not exhibit strong aggregation, the water-soluble fractions of dimers or oligomers do not exhibit pronounced fluorescence quenching.

3.1.2.2. m-THPP and m-THPC. The capacity of KP micelles for solubilizing m-THPP and m-THPC is clearly lower than for Ce6 derivatives. The averaged τ_{av} -values indicate multiple components including monomers, more prevalent at 1 μ M, coexisting with oligomers and higher aggregates, mainly at 100 μ M (Fig. 3). This agrees with previous results that have shown a limited capability specifically of KP micelles for encapsulating hydrophobic PSs with larger log*P* values ($\sim > 5$) [34,61]. On the other hand, in PVP, long fluorescence lifetimes of about 10 ns that were constant over time at a concentration of 100 μ M suggest that both PSs are associated with PVP as monomers. This demonstrates that PVP covers a wide range from hydrophilic to hydrophobic compounds as delivery system with high versatility [40].

3.2. Fluorescence Lifetime Imaging Microscopy of PSs in Cells

Based on the results obtained for the single PSs and their combinations with carrier systems in solution, the subsequent aim was to study their decay dynamics in the complex environment of model cancer cells. For this, HeLa cells were incubated with the PSs SerCe, Ce4, CeDME, m-THPC, and m-THPP (Fig. 1) either alone or encapsulated into micelles consisting of KP or RH (used for CeDME, Fig. 2) or into PVP. The incubation time was 3 h, 12 h, and 24 h while the total duration of cell growth in culture was kept constant (Fig. S6). After removal of the

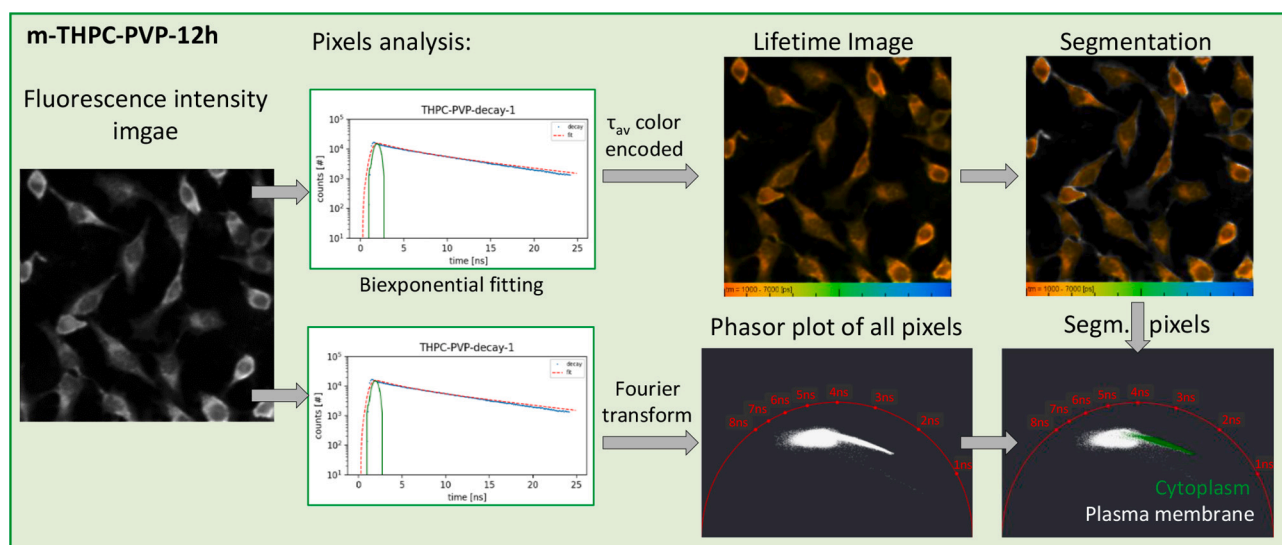


Fig. 4. Workflow shown for an example of HeLa cells that were incubated for 12 h with m-THPC-PVP. Single pixels of the fluorescence intensity image were analyzed by plotting (photon counts versus time) and fitting the decay curves with a bi-exponential function. Lifetime images are created by colour-encoding the weighted average τ -values from the fits. Phasor plots are obtained by Fourier transformations of single pixels and image segmentation separates pixels originating from the plasma membrane (white) and the cytoplasm (green). (For interpretation of the references to colour in this figure legend, the reader is referred to the web version of this article.)

incubation media and washing steps fluorescence intensity images of the cells were recorded. Fig. 4 depicts the workflow that was applied for fluorescence analysis on each of the samples. The time-resolved fluorescence decay curves were measured for each pixel and analyzed in two different modes: (1) From bi-exponential fitting, the weighted average lifetime was calculated and colour-encoded to obtain the fluorescence lifetime images; (2) From Fourier transformation of the single pixel fluorescence decays, phasor plots were created. In addition, the fluorescence images were segmented into pixels deriving from the plasma membrane and pixels deriving from the cytoplasm. The two different compartments were in turn colour-encoded on the pixel clouds in the phasor plots. This allows direct visualization and identification of different populations distinguished by their lifetimes.

The phasor approach results in a polar plot, in which each pixel of the fluorescence image is represented by a point (phasor) that is displayed in the universal circle. For mono-exponential decays, the phasor is located on the semi-circle, and for multi-exponential decays, the phasor coordinates derive from a linear combination of the weighted single lifetimes and the phasor is located inside the universal circle as shown in the example of Fig. 4 [42,68]. According to the fluorescence intensity images (Figs. S7 and S8), all PSs examined here, either pure or associated with micelles or PVP, were internalized into HeLa cells and localized in the cell membrane or cytoplasm excluding the nucleus, as exemplified for m-THPC-PVP in Fig. 4. The corresponding lifetime images are displayed in Figs. S9 and S10.

3.2.1. Phasor Analysis of Fluorescence Decays after 3 H and 24 H Incubation

In Figs. 5 and 6, the phasor plots are shown obtained from the fluorescence lifetime decay data of HeLa cells exposed to the PSs with and without carriers during 3 h and 24 h, respectively. The first column refers to PSs applied without carrier, and the second and third columns refer to PSs applied with micelles and with PVP. White pixel clouds originate from the plasma membrane and green pixel clouds from the cytoplasm compartments.

The PSs can be classified into three groups (I – III) according to their intracellular fluorescence lifetimes, i.e., to the position of the pixel clouds in the phasor space and their time evolution: (I) SerCe; (II) Ce4/CeDME, and (III) m-THPC/m-THPP. This classification coincides with

the logP value ranges and substitution pattern of the PSs and will be outlined in further detail below.

3.2.1.1. (I) SerCe. Circular pixel clouds located inside the semicircle were obtained for SerCe under each condition (carrier/no carrier, short and long incubation time). This indicates that multiple states of intracellular SerCe with different fluorescence lifetimes exist. In accordance with the solution data (Fig. 3), encapsulation of SerCe into micelles or PVP did not lead to considerable fluorescence lifetime changes. This was mainly attributed to the fact that this chlorin is rather hydrophilic and has relatively good water solubility at low concentrations where mono-, di-, or oligomers are formed. This means that upon carrier encapsulation of SerCe the average fluorescence lifetime is not expected to be strongly altered by disaggregation processes. In contrast, in the cellular environment, contributions from short-lived components must be responsible for the shift of the pixel cloud into the inner circle. This shift is slightly more pronounced for the cytoplasm compartment colored green in the phasor plots (Figs. 5, 6) than for the outer cell membrane region (colored white). Since SerCe has only a low tendency to form large aggregates, short-lived components most likely emerge from its specific microenvironment in the cell or from interaction of the chlorin with cellular components located in the cytoplasm and in or on the cell membrane.

3.2.1.2. Cell Uptake Mechanism of Free SerCe. For free porphyrinic PSs, cell uptake mechanisms and intracellular localization depend on their substitution patterns, which in turn determine amphiphilicity, charge, overall hydrophilicity, and the logP value [18,69]. Accordingly, amphiphilicity promotes membrane insertion [70,71] but decreases passive trans-membrane diffusion. Highly hydrophilic PSs reportedly enter cells mainly via the endocytic route by pinocytosis where the PS is internalized in the solute [72]. This route typically leads to a subsequent lysosomal deposition as depicted in Fig. 7 A (route 1) and applies most likely for SerCe.

The lower pH value in lysosomes (pH 4.0–5.5) [72] compared to the cytosol has been recently postulated to cause decreased fluorescence lifetimes of radachlorin, a PS mixture mainly consisting of Ce6, in different cell types including HeLa cells [31]. The endocytic cell uptake pathway has also been proposed for anionic sulfonated aluminum

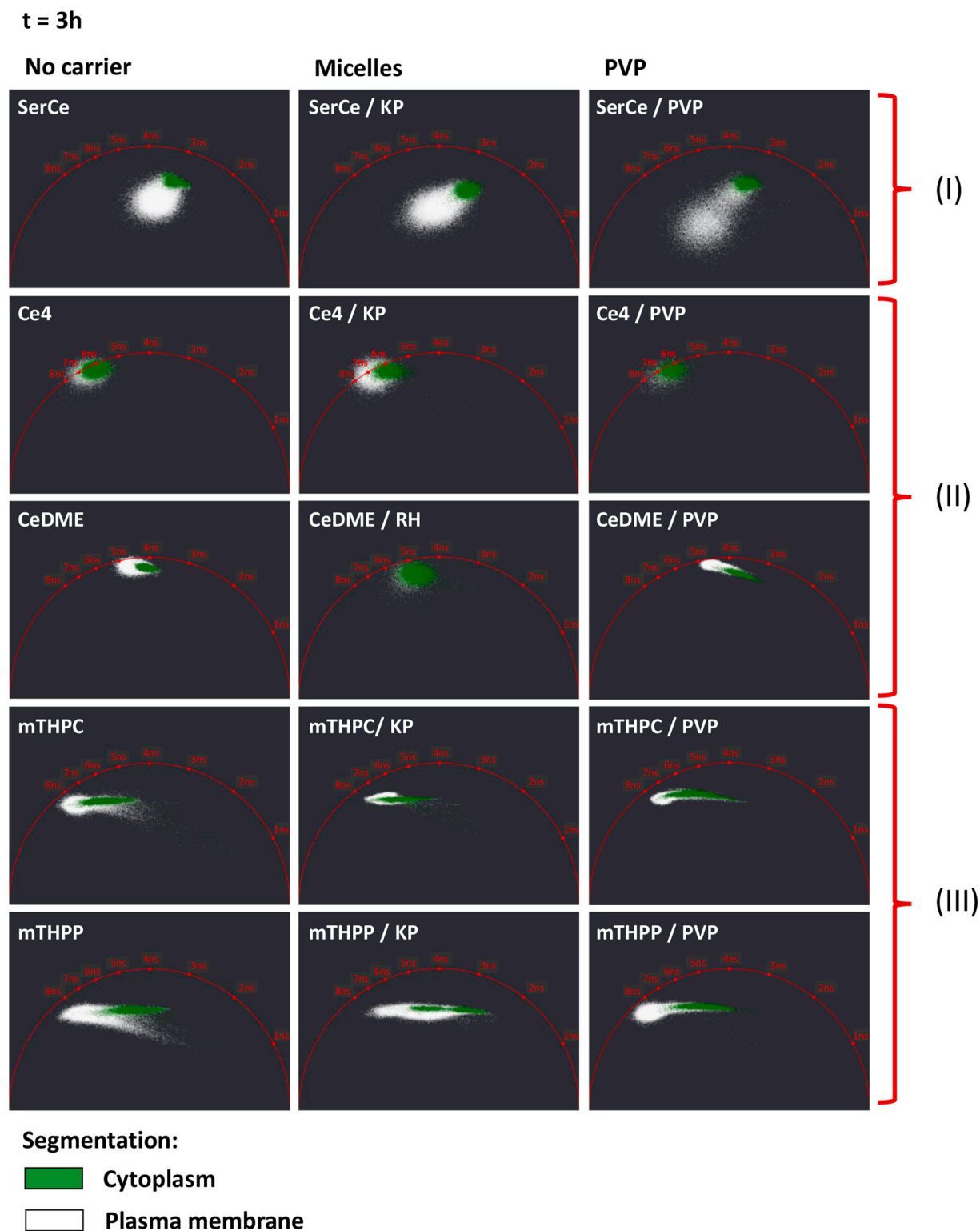


Fig. 5. Phasor plots calculated from segmented FLIM images of HeLa cells incubated for 3 h with SerCe, Ce4, CeDME, m-THPC and m-THPP without carrier (first column), encapsulated into micelles (second column), and encapsulated into PVP (third column). Pixel clouds originating from the plasma membrane are colored in white and pixel clouds originating from the cytoplasm are colored green. (For interpretation of the references to colour in this figure legend, the reader is referred to the web version of this article.)

phthalocyanine (AlPcS₂) that likewise exhibited intracellular reduced fluorescence lifetime possibly also related to lysosomal localization [33]. Since SerCe has three ionizable carboxylate groups, the same localization- and pH-dependence for its fluorescence lifetime may hold. The pK_a values of Ce6 derivatives with at least three carboxylate groups

typically lie above 4 [73], so that they will be protonated in the lysosomal space. This in turn reduces hydrophilicity and promotes aggregate formation. Slow release of the PS from the lysosomes into the cytosol over time may account for the shift of the phasor cloud towards longer lifetimes after 24 h (Fig. 6).

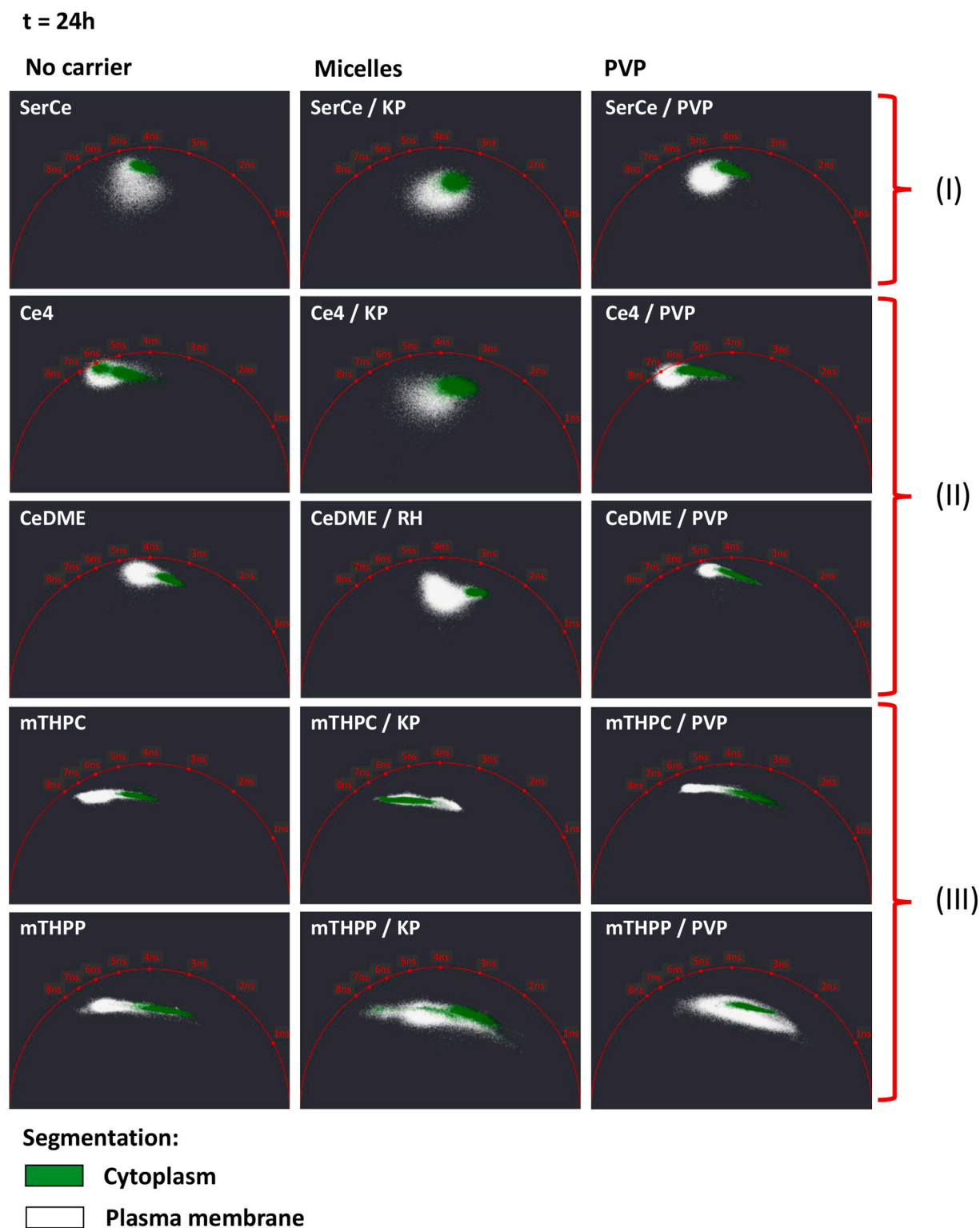


Fig. 6. Phasor plots calculated from segmented FLIM images of HeLa cells incubated for 24 h with SerCe, Ce4, CeDME, m-THPC and m-THPP without carrier (first column), encapsulated into micelles (second column), and encapsulated into PVP (third column). Pixel clouds originating from the plasma membrane are colored in white and pixel clouds originating from the cytoplasm are colored green. (For interpretation of the references to colour in this figure legend, the reader is referred to the web version of this article.)

3.2.1.3. (II) Ce4, CeDME. Ce4 and CeDME are amphiphilic with two and one ionizable carboxylate groups on one side of the chlorin macrocycle, respectively (Fig. 1). Their calculated $\log P$ values are similar with 4.64 for Ce4 and 4.68 for CeDME (Table 1) [52]. Both PSs show aggregation in aqueous solution that is — compared to Ce4 — more

pronounced for CeDME with an onset concentration of $\sim 1 \mu\text{M}$ [61].

The intracellular fluorescence lifetime properties of Ce4 and CeDME gave rise to similar patterns in the phasor plots (Figs. 5 and 6). Noticeably, after 3 h incubation of cells with Ce4, the phasors cluster on the edge of the universal cycle independent of the formulation applied, i.e.,

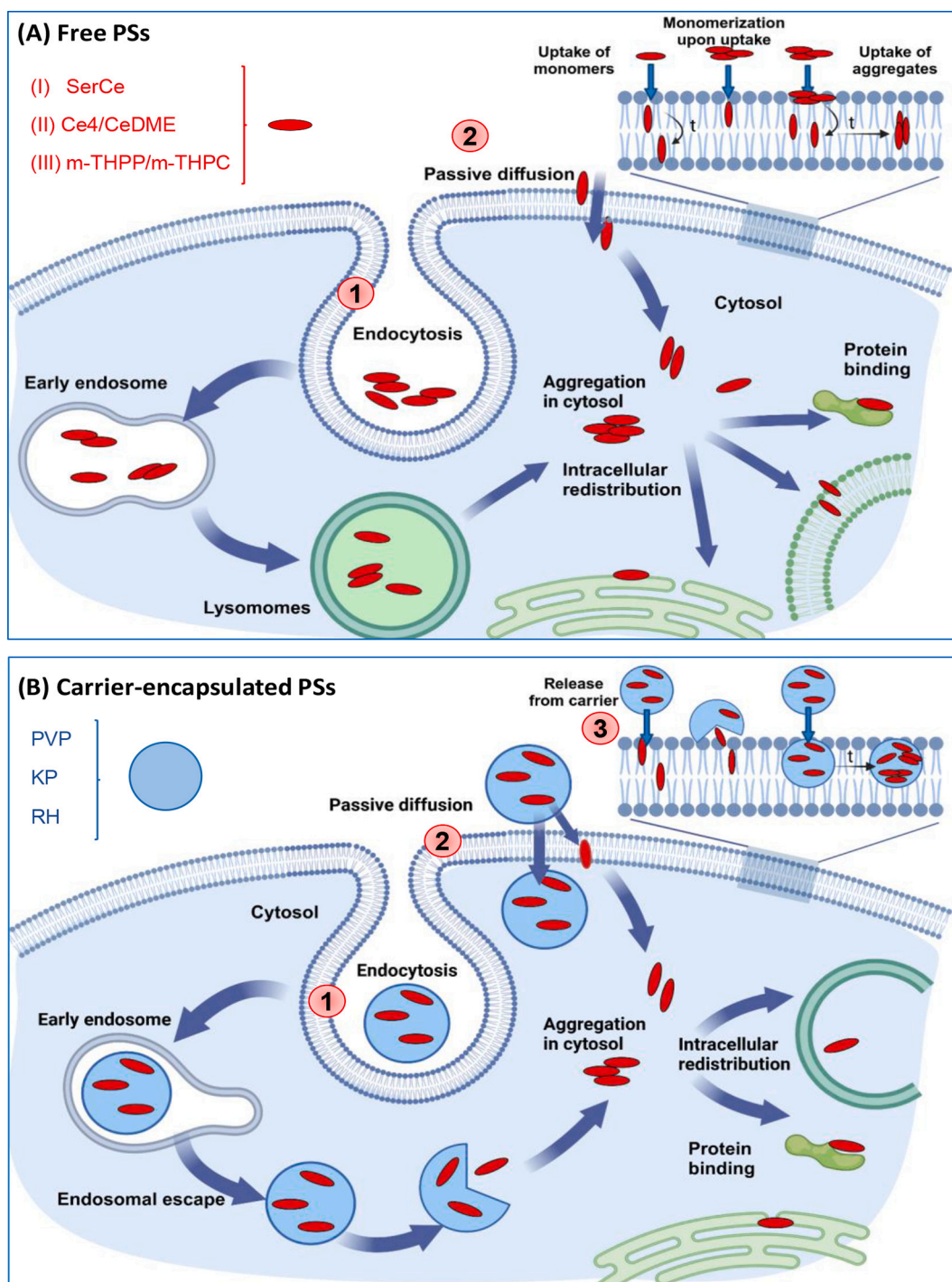


Fig. 7. Scheme for proposed cell uptake pathways and intracellular localization and processes for (A) free PSs and (B) PSs encapsulated into carriers. Alternative cell uptake routes are numbered 1 for endocytosis, 2 for passive diffusion, and 3 for direct release of the PS from the carrier into the plasma membrane. Created with BioRender.com.

for Ce4 in its free form, associated with KP-micelles or PVP (Fig. 5). This indicates that in all three cases predominantly monomeric species of Ce4 with mono-exponential fluorescence emission decays exist. Moreover, intracellular Ce4 exhibits a fluorescence lifetime of 6–7 ns, which is longer than in ethanol solution (Table 1). Pixel clouds of both compartments, the plasma membrane, and the cytoplasm, overlap except for micelles where a slight shift towards the inside of the universal circle appears. The phasors for CeDME are not exactly on but very close to the universal circle in the phasor plots for 3 h cell incubation (Fig. 5). Like for Ce4, this suggests a predominant monomeric population for pure as

well as for carrier associated CeDME.

3.2.1.4. Cell Uptake Mechanism of free Ce4/CeDME. As stated above, amphiphilicity promotes interactions with membranes. Depending on the $\log P$ value of the amphiphilic PS it can pass the membrane by passive diffusion that may involve a flip-flop mechanism, which takes place very slowly so that the PS can reside a long time in the membrane [73,74]. Our previous studies could detect membrane localization of Ce4 in HeLa cells with atomic resolution applying high resolution magic angle spinning (HR-MAS) NMR spectroscopy. The NMR data of HeLa cells

incubated with Ce4 revealed concentration dependent interaction with cellular phospholipid head-groups [15]. It can thus be assumed that Ce4 and CeDME enter the cells mainly via passive diffusion, as depicted in Fig. 7A (route 2), upon which the PS resides in monomeric form reaching into the hydrophobic membrane core region, accounting for the long-lived species.

3.2.1.5. Changes Appearing Over Time (24 h). Following 24 h cell incubation with Ce4 or CeDME, the pixel clouds in the Phasor plots move towards the interior of the universal circle (Fig. 6). This is most pronounced for the PS formulation with micellar carriers (KP and RH). Thus, the homogeneous, mainly monomeric species observed after 3 h become heterogeneous indicating a mixture of components with mono-, bi-, or multi-exponential fluorescence decay curves. In addition, the pixel clouds associated with the plasma membrane (white) and the cytoplasm (green) move apart and appear more separated in the phasor plots after 24 h. There is a clear trend towards shorter lifetimes in the cytoplasmic compartment. This suggests that the long-lived components are better stabilized over time in the plasma membrane. If the PS is released into the cytosol, aggregation can take place (Fig. 7A) and account for an increase in short-lived components. As discussed above for SerCe, interaction with cellular components and localization in specific organelles like lysosomes in the cytoplasm potentially contribute to the PS population with short lifetime values.

3.2.1.6. PVP Versus Micelles. In comparison, there is a clear difference after 24 h between micellar systems and PVP. When applied with PVP, the pixel clouds for Ce4 and CeDME remain on or close to the edge of the semi-circle in the Phasor plots for the plasma membrane compartment. Accordingly, PVP is capable to stabilize the monomeric species with a long fluorescence lifetime in the cell even after 24 h. Strong binding of the Ce6 derivatives to PVP may be responsible for this behavior and suggests that a large part of the PS remains associated with its carrier inside the cell. This is in agreement with previous studies indicating that Ce4 remains largely associated with PVP after efficient uptake into HeLa cells. This was concluded from the observation that PVP reduced direct Ce4-membrane interaction and significantly attenuated the cell metabolic response to Ce4 [15]. On the contrary, PEG-PPG block-copolymer and Cremophor micelles are carriers with enhanced internal motional freedom of the encapsulated drug allowing faster release [6,66,67] and consequently aggregate formation in the cytosol.

3.2.1.7. (III) m-THPC, m-THPP. Compared to the Ce6 derivatives, m-THPP and m-THPC have distinguished structural properties: First, the symmetric substitution pattern reduces amphiphilicity and may thus hamper monomeric insertion into membrane bilayers. Second, the relatively high $\log P$ values (Table 1) promote aggregate formation in aqueous media as already demonstrated for the corresponding compounds in solution.

In the phasor plots of m-THPP and m-THPC, elongated pixel clouds in the interior of the universal circle form a common feature (Figs. 5 and 6). Moreover, in none of the applied conditions, a pure monomeric population was present. Nevertheless, a considerable fraction of long-lived species exists after 3 h incubation time for the carrier-free and PVP-associated systems, in particular for m-THPP-PVP where the pixel cluster lies close to the universal circle for the plasma membrane compartment (Fig. 5). For these systems (free/PVP), the cytoplasm compartment is always marked by larger contributions from short-lived components. Similarly, a long incubation time of 24 h leads to an overall shift of the pixel clusters towards shorter lifetimes. In accordance with these data, time-dependent intracellular fluorescence lifetime shortening of m-THPC has been previously reported and was mainly attributed to the formation of aggregates that predominate after 24 h in the cytoplasm [29]. In addition, photobleaching of m-THPC may contribute to lifetime shortening [33,75,76]. When applied with micelles, the

phasor plots for m-THPP and m-THPC reflect the presence of heterogeneous lifetime distributions for both compartments already after 3 h incubation without further significant changes after 24 h.

3.2.1.8. Cell Uptake Mechanism of Free m-THPC/m-THPP. In contrast to the short average lifetimes of free m-THPP and m-THPC determined in aqueous solutions (Fig. 3), the weighted average lifetime of the same carrier-free compounds in the cellular environment is clearly longer with contributions from τ -values >8 ns as indicated by the corresponding phasor positions near the universal circle. Since these contributions derive from the plasma membrane compartment, localization of the PSs in the hydrophobic region of the phospholipid bilayers is conceivable. For free m-THPC, passive diffusion across the plasma membrane (Fig. 7A) is reported to be the main cell uptake pathway [77,78]. Moreover, studies have indicated that m-THPC uptake can take place in aggregated form (Fig. 7A) with subsequent monomerization upon entering the cell [79,80]. This would explain the results found in the present work, i.e., the emergence of long-lived (monomeric) m-THPC/THPP species when cells were incubated with the free PSs and the simultaneous presence of short-lived (aggregated) species in the plasma membrane. In accordance with these findings, it has been previously reported that very hydrophobic strongly aggregating Ce6-derivatives exhibited partial intracellular disaggregation that correlated with the extent of hydrophobicity. In this study, uptake of large aggregates was proposed by endocytosis [30].

3.2.1.9. PVP Versus Micelles. Like for Ce4/CeDME, strong binding to PVP may also account for a relatively large fraction of long-lived monomeric m-THPP and m-THPC. The impact of PVP onto the fluorescence lifetime was demonstrated by the data obtained in solution (Fig. 3). Since passive diffusion is a proposed cell uptake pathway for small NPs including PVP (MW of 10 kDa applied here) [81], PVP loaded particles are likely to reside in the plasma membrane. Only a slow release into the cytoplasm may lead to the appearance of short-lived components in the cytoplasm and an overall spread after 24 h.

The mechanism how poloxamer micelles enter cells is not yet fully understood and several routes have been proposed that may coexist (Fig. 7B, routes 1–3). They include endocytosis of the whole particles, passive diffusion of small particles, decomposition of the micelles upon cell entry, and release of the encapsulated drug at the cell membrane [82,83]. Previously, we were able to detect intracellular micelles and building blocks thereof following HeLa cell incubation with KP micelles [15]. In any case, structural and binding properties of each drug-carrier system are crucial factors that determine the effective route(s). Therefore, m-THPC/m-THPP formulation in poloxamer micelles may—at least in part—redirect the cell uptake to the endocytic pathway [84]. This reduces direct deposition of PS monomers into the plasma membrane. In addition, the binding affinity between m-THPC/m-THPP and KP micelles is rather low as was indicated by the fluorescence lifetime data in solution. Similar like for Ce4/CeDME but more pronounced, release from micelles into the cytoplasm promotes aggregate formation and possible redistribution to different organelles, among which ER and the Golgi apparatus are proposed preferential localization sites of m-THPC in cells [85].

3.2.2. Summary: Impact of Carriers and of Cell Uptake Pathways

3.2.2.1. In Solution. The solution data have shown that PS aggregation leads to fluorescence lifetime shortening that in turn depends on the extent of aggregate formation, i.e., if dimers, oligomers, or polymers are formed. Insertion into polymeric carriers leads to monomerization of the PSs and can thus maintain or reinstall a long-lived monomeric species. The fluorescence lifetimes measured in carrier systems depend on the polarity of the carrier microenvironment and on the binding strength. Binding to PVP is strong whereas micellar carriers allow exchange with

the aqueous medium to different extents. The equilibrium of this exchange process is governed by the $\log P$ value of the PS.

3.2.2.2. Inside Cells. In the cellular environment monomeric PS species with long lifetimes exist if they are (i) not strongly aggregating in the cytosol like SerCe, (ii) localize in the hydrophobic region of cell membranes (Ce4/CeDME and m-THPP/m-THPC), or (iii) remain associated with their carrier (mainly PVP) in the monomeric form inside the cell where strong binding to the carrier is advantageous.

In the cellular environment PS species with short lifetimes emerge if they are (i) released from the plasma membrane, endosomes, or carriers into the cytosol where aggregation takes place over time, (ii) localized in cell compartments with a lower pH value like lysosomes, (iii) interact with cellular components like specific proteins (Fig. 7), or (iv) photobleaching products with short fluorescence lifetimes are formed. Moreover, the strong tendency to form aggregates may also lead over time to the formation of oligomers inside the membrane (Fig. 7 A) or inside micelles with sufficient internal flexibility.

3.2.2.3. Cell Uptake Pathways. Cell uptake pathways play a major role for the intracellular fate of the PS and its fluorescence properties. For the pure PSs, passive diffusion through the membrane enables the PS to reside in the membrane in its monomeric form (class II and III PSs). The endocytic pathway of hydrophilic PS (class I) replaces membrane insertion and leads among other organelles in lysosomal localization (Fig. 7A).

Cell internalization of micelles and PVP takes place via passive diffusion and/or via the endocytic pathway (Fig. 7B). The size of the carriers can strongly affect the cellular uptake pathway and small particles including PVP with a MW of 10 kDa used in this study are capable to enter the cell via passive diffusion [81]. For the less rigid micelles, several cell entry routes may coexist including direct drug release into the plasma membrane (Fig. 7B) [82,83]. Moreover, it is conceivable that – depending on the binding strength between drug and polymer – at least a portion of the porphyrinic compound can already be released before entering the cell in its encapsulated form.

4. Conclusion

Efficient PDT relies on the monomeric state and optimal photo-physical properties of a given PS in the target tissue. Monitoring the intracellular fluorescence lifetime provides a meaningful measure to assess the performance of the PS directly in the physiological environment. Only long fluorescence lifetimes will allow efficient conversion to triplet states of the PS required for the phototoxic reaction.

In the current study, the FLIM Phasor approach was applied to analyze the intracellular fluorescence lifetime distribution of five different PSs in their free and carrier-associated forms. The findings demonstrate that even hydrophobic PSs that exhibit pronounced aggregation in aqueous media can be disaggregated upon interacting with cell membranes and thus unfold their PDT efficiency. On the other hand, water-soluble, hydrophilic anionic PSs may suffer from partial loss of their phototoxic potential upon cell uptake via endocytosis due to lysosomal localization and/or interaction with cytosolic components, i. e., processes that may lead to fluorescence quenching.

To date, only few studies have addressed the impact of carriers on the intracellular emission lifetime distribution of PSs. Our results have shown that drug carrier systems with high binding affinity can maintain the monomeric state of the PS inside the cell over prolonged time. The time interval shortens with decreasing binding strength leading to drug release into the cytosol where aggregation takes place. In this respect, PVP turned out to be a more efficient carrier than the rather flexible micelles. However, micellar carriers are tunable in size and composition for improved drug binding. Therefore, it would be interesting for future studies — in particular for hydrophobic PSs like m-THPP/m-THPC — to

probe further block copolymer micelles with lower HLB values (hydrophilic-lipophilic balance) or self-emulsifying micelles like RH that have higher lipophilic capacity [34]. For hydrophilic PSs, the carrier does not make a big difference on the cellular level, whereas it remains important for protecting the PS during its transport in the bloodstream and for enhancing its uptake into tumor tissue.

The results reported here can contribute to optimize PDT treatment conditions, e.g., by estimating the optimal therapeutic time window between PS application and light activation. Moreover, the design of efficient PS-carrier systems should be governed by high affinity of the PS for binding to the carrier and cell membranes.

Funding

This work was supported by the Swiss National Science Foundation [SNSF grant number 205320–179038].

CRediT authorship contribution statement

Florentin S. Spadin: Writing – review & editing, Visualization, Methodology, Investigation, Formal analysis. **Lea P. Gergely:** Writing – review & editing, Investigation. **Tobias Kämpfer:** Writing – review & editing, Investigation. **Martin Frenz:** Conceptualization, Supervision, Funding acquisition, Writing – review & editing. **Martina Vermathen:** Conceptualization, Formal analysis, Supervision, Visualization, Writing – original draft.

Declaration of Competing Interest

The authors declare that they have no known competing financial interests or personal relationships that could have appeared to influence the work reported in this paper.

Data availability

Data will be made available on request.

Acknowledgement

The authors thank Prof. Jean-Marc Nuoffer for providing support in the cell culture work performed at the Center for Laboratory Medicine, Inselspital Bern.

Appendix A. Supplementary data

The supplementary material contains fluorescence decay curves of the photosensitizers in solution in the absence and presence of carriers (Figs. S1 – S5), a cell incubation scheme applied in the current work (Fig. S6), fluorescence intensity images of HeLa cells after incubation with the photosensitizers free or encapsulated in carriers (Figs. S7 and S8), and fluorescence lifetime images of HeLa cells after incubation with the photosensitizers free or encapsulated in carriers (Figs. S9 and S10). Supplementary data to this article can be found online at [<https://doi.org/10.1016/j.jphotobiol.2024.112904>].

References

- [1] A. Akbar, S. Khan, T. Chatterjee, M. Ghosh, Unleashing the power of porphyrin photosensitizers: illuminating breakthroughs in photodynamic therapy, *J. Photochem. Photobiol. B* 248 (2023) 112796, <https://doi.org/10.1016/j.jphotobiol.2023.112796>.
- [2] J.F. Lovell, P.C. Lo, Porphyrins and phthalocyanines for theranostics, *Theranostics* 2 (2012) 815–816, <https://doi.org/10.7150/thno.5128>.
- [3] J.M. Dąbrowski, L.G. Arnaut, Photodynamic therapy (PDT) of cancer: from local to systemic treatment, *Photochem. Photobiol. Sci.* 14 (2015) 1765–1780, <https://doi.org/10.1039/C5PP00132C>.

- [4] P.G. Seybold, M. Gouterman, Porphyrins., XIII: fluorescence spectra and quantum yields, *J. Mol. Spectrosc.* 31 (1969) 1–13, [https://doi.org/10.1016/0022-2852\(69\)90335-x](https://doi.org/10.1016/0022-2852(69)90335-x).
- [5] E.F.F. Silva, F.A. Schaberle, C.J.P. Monteiro, J.M. Dąbrowski, L.G. Arnaut, The challenging combination of intense fluorescence and high singlet oxygen quantum yield in photostable chlorins – a contribution to theranostics, *Photochem. Photobiol. Sci.* 12 (2013) 1187–1192, <https://doi.org/10.1039/C3PP25419D>.
- [6] I. Gjuroski, E. Girousi, C. Meyer, D. Hertig, D. Stojkov, M. Fux, N. Schnidrig, J. Bucher, S. Pfister, L. Sauser, H.-U. Simon, P. Vermathen, J. Furrer, M. Vermathen, Evaluation of polyvinylpyrrolidone and block copolymer micelle encapsulation of serine chlorin e6 and chlorin e4 on their reactivity towards albumin and transferrin and their cell uptake, *J. Control. Release* 316 (2019) 150–167, <https://doi.org/10.1016/j.jconrel.2019.10.010>.
- [7] P.S. Maharjan, H.K. Bhattarai, Singlet oxygen, photodynamic therapy, and mechanisms of Cancer cell death, *J. Oncol.* 2022 (2022) 7211485, <https://doi.org/10.1155/2022/7211485>.
- [8] A.P. Castano, T.N. Demidova, M.R. Hamblin, Mechanisms in photodynamic therapy: part three-photosensitizer pharmacokinetics, biodistribution, tumor localization and modes of tumor destruction, *Photodiagn. Photodyn. Ther.* 2 (2005) 91–106, [https://doi.org/10.1016/s1572-1000\(05\)00060-8](https://doi.org/10.1016/s1572-1000(05)00060-8).
- [9] G.J. Smith, The effects of aggregation on the fluorescence and the triplet state yield of hematoporphyrin, *Photochem. Photobiol.* 41 (1985) 123–126, <https://doi.org/10.1111/j.1751-1097.1985.tb03459.x>.
- [10] D. Phillips, A lifetime in photochemistry; some ultrafast measurements on singlet states, *Proc. R Soc. A: Math.* 472 (2016) 20160102, <https://doi.org/10.1098/rspa.2016.0102>.
- [11] S. Li, F. Yang, Y. Wang, T. Du, X. Hou, Emerging nanotherapeutics for facilitating photodynamic therapy, *J. Chem. Eng.* 451 (2023) 138621, <https://doi.org/10.1016/j.cej.2022.138621>.
- [12] S.S. Lucky, K.C. Soo, Y. Zhang, Nanoparticles in photodynamic therapy, *Chem. Rev.* 115 (2015) 1990–2042, <https://doi.org/10.1021/cr5004198>.
- [13] N. Hoshyar, S. Gray, H. Han, G. Bao, The effect of nanoparticle size on in vivo pharmacokinetics and cellular interaction, *Nanomedicine (London)* 11 (2016) 673–692, <https://doi.org/10.2217/nmm.16.5>.
- [14] L.C. Nelemans, L. Gurevich, Drug delivery with polymeric Nanocarriers-cellular uptake mechanisms, *Materials (Basel)* 13 (2020) 366, <https://doi.org/10.3390/ma13020366>.
- [15] M. Vermathen, T. Kämpfer, J.M. Nuoffer, P. Vermathen, Intracellular fate of the photosensitizer Chlorin e4 with different carriers and induced metabolic changes studied by ¹H NMR spectroscopy, *Pharmaceutics* 15 (2023), <https://doi.org/10.3390/pharmaceutics15092324>.
- [16] D. Kessel, Correlation between subcellular localization and photodynamic efficacy, *J. Porphyrins Phthalocyanines* 8 (2004) 1009–1014, <https://doi.org/10.1142/S1088424604000374>.
- [17] N.N. Peskova, A.A. Brilkina, A.A. Gorokhova, N.Y. Shilyagina, O.M. Kutova, A. S. Nerush, A.G. Orlova, L.G. Klapshina, V.V. Vodeneev, I.V. Balalaeva, The localization of the photosensitizer determines the dynamics of the secondary production of hydrogen peroxide in cell cytoplasm and mitochondria, *J. Photochem. Photobiol. B Biol.* 219 (2021) 112208, <https://doi.org/10.1016/j.jphotobiol.2021.112208>.
- [18] A.P. Castano, T.N. Demidova, M.R. Hamblin, Mechanisms in photodynamic therapy: part one-photosensitizers, photochemistry and cellular localization, *Photodiagn. Photodyn. Ther.* 1 (2004) 279–293, [https://doi.org/10.1016/S1572-1000\(05\)00007-4](https://doi.org/10.1016/S1572-1000(05)00007-4).
- [19] M.Y. Berezin, S. Achilefu, Fluorescence lifetime measurements and biological imaging, *Chem. Rev.* 110 (2010) 2641–2684, <https://doi.org/10.1021/cr900343z>.
- [20] K. Awasthi, D. Moriya, T. Nakabayashi, L. Li, N. Ohta, Sensitive detection of intracellular environment of normal and cancer cells by autofluorescence lifetime imaging, *J. Photochem. Photobiol. B Biol.* 165 (2016) 256–265, <https://doi.org/10.1016/j.jphotobiol.2016.10.023>.
- [21] R. Datta, T.M. Heaster, J.T. Sharick, A.A. Gillette, M.C. Skala, Fluorescence lifetime imaging microscopy: fundamentals and advances in instrumentation, analysis, and applications, *J. Biomed. Opt.* 25 (2020) 1–43, <https://doi.org/10.1117/1.Jbo.25.7.071203>.
- [22] A.S.-C. Yeh, S.M. Patterson, E.J. Hayward, Q. Fang, Time-Resolved Fluorescence in Photodynamic Therapy, *Photonics* 1 (2014) 530–564, <https://doi.org/10.3390/photonics1040530>.
- [23] A. Bitton, J. Sambrano, S. Valentino, J.P. Houston, A review of new high-throughput Methods designed for fluorescence lifetime sensing from cells and tissues, *Front. Phys.* 9 (2021), <https://doi.org/10.3389/fphy.2021.648553>.
- [24] A. Rück, F. Dolp, C. Hülshoff, C. Hauser, C. Scalfi-Happ, Fluorescence lifetime imaging in PDT. An overview, *Med. Laser Applicat.* 20 (2005) 125–129, <https://doi.org/10.1016/j.mla.2005.03.009>.
- [25] J.A. Russell, K.R. Diamond, T.J. Collins, H.F. Tiedje, J.E. Hayward, T.J. Farrell, M. S. Patterson, Q.Y. Fang, Characterization of fluorescence lifetime of Photofrin and delta-aminolevulinic acid induced protoporphyrin IX in living cells using single- and two-photon excitation, *IEEE J. Sel. Top. Quant.* 14 (2008) 158–166, <https://doi.org/10.1109/JSTQE.2007.912896>.
- [26] A. Rueck, F. Dolp, C. Huelshoff, C. Hauser, C. Scalfi-Happ, FLIM and SLIM for molecular imaging in PDT, in: *SPIE-Int Soc Optical Engineering: Bellingham vol. 5700*, 2005.
- [27] S.C. Yeh, K.R. Diamond, M.S. Patterson, Z. Nie, J.E. Hayward, Q. Fang, Monitoring photosensitizer uptake using two photon fluorescence lifetime imaging microscopy, *Theranostics* 2 (2012) 817–826, <https://doi.org/10.7150/thno.4479>.
- [28] M. Kress, T. Meier, R. Steiner, F. Dolp, R. Erdmann, U. Ortmann, A. Rück, Time-resolved microspectrofluorometry and fluorescence lifetime imaging of photosensitizers using picosecond pulsed diode lasers in laser scanning microscopes, *J. Biomed. Opt.* 8 (2003) 26–32, <https://doi.org/10.1117/1.1528595>.
- [29] H.P. Lassalle, M. Wagner, L. Bezdetnaya, F. Guillemin, H. Schneckenburger, Fluorescence imaging of Foscan (R) and Foslip in the plasma membrane and in whole cells, *J. Photochem. Photobiol. B Biol.* 92 (2008) 47–53, <https://doi.org/10.1016/j.jphotobiol.2008.04.007>.
- [30] L. Kelbaskaus, W. Dietel, Internalization of aggregated photosensitizers by tumor cells: subcellular time-resolved fluorescence spectroscopy on derivatives of pyropheophorbide-a ethers and chlorin e6 under femtosecond one- and two-photon excitation, *Photochem. Photobiol.* 76 (2002) 686–694, [https://doi.org/10.1562/0031-8655\(2002\)076<0686:ioapbt>2.0.co;2](https://doi.org/10.1562/0031-8655(2002)076<0686:ioapbt>2.0.co;2).
- [31] A.V. Belashov, A.A. Zhikhoreva, A.V. Salova, T.N. Belyaeva, I.K. Litvinov, E. S. Kornilova, I.V. Semenova, O.S. Vasyutinskii, Analysis of Radachlorin localization in living cells by fluorescence lifetime imaging microscopy, *J. Photochem. Photobiol. B Biol.* 243 (2023) 112699, <https://doi.org/10.1016/j.jphotobiol.2023.112699>.
- [32] A.D. Scully, R.B. Ostler, D. Phillips, P. O'Neill, K.M.S. Townsend, A.W. Parker, A. J. MacRobert, Application of fluorescence lifetime imaging microscopy to the investigation of intracellular PDT mechanisms, *Bioimaging* 5 (1997) 9–18, [https://doi.org/10.1002/1361-6374\(199703\)5:1](https://doi.org/10.1002/1361-6374(199703)5:1).
- [33] J.P. Connelly, S.W. Botchway, L. Kunz, D. Pattison, A.W. Parker, A.J. MacRobert, Time-resolved fluorescence imaging of photosensitizer distributions in mammalian cells using a picosecond laser line-scanning microscope, *J. Photochem. Photobiol. A Chem.* 142 (2001) 169–175, [https://doi.org/10.1016/S1010-6030\(01\)00511-1](https://doi.org/10.1016/S1010-6030(01)00511-1).
- [34] L.P. Gergely, C. Yüceel, Ü. İsci, F.S. Spadin, L. Schneider, B. Spingler, M. Frenz, F. Dumoulin, M. Vermathen, Comparing PVP and polymeric micellar formulations of a PEGylated photosensitizing Phthalocyanine by NMR and optical techniques, *Mol. Pharm.* 20 (2023) 4165–4183, <https://doi.org/10.1021/acs.molpharmaceut.3c00306>.
- [35] W. Akers, F. Lesage, D. Holten, S. Achilefu, In vivo resolution of multiexponential decays of multiple near-infrared molecular probes by fluorescence lifetime-gated whole-body time-resolved diffuse optical imaging, *Mol. Imaging* 6 (2007) 237–246, <https://doi.org/10.2310/7290.2007.00020>.
- [36] A.V. Belashov, A.A. Zhikhoreva, S.S. Kruglov, A.V. Panchenko, I.V. Semenova, O. S. Vasyutinskii, Analysis of in vivo Radachlorin accumulation through FLIM-assisted examination of ex vivo histological samples, *Photonics* 9 (2022) 711, <https://doi.org/10.3390/photonics9100711>.
- [37] A. Battisti, P. Morici, A. Sgarbossa, Fluorescence lifetime imaging microscopy of Porphyrins in helicobacter pylori biofilms, *Pharmaceutics* 13 (2021), <https://doi.org/10.3390/pharmaceutics13101674>.
- [38] K. Awasthi, K. Yamamoto, K. Furuya, T. Nakabayashi, L. Li, N. Ohta, Fluorescence characteristics and lifetime images of photosensitizers of talaporfin sodium and sodium pheophorbide a in normal and cancer cells, *Sensors* 15 (2015) 11417–11430, <https://doi.org/10.3390/s150511417>.
- [39] A. Wiehe, M.O. Senge, The photosensitizer Temporfin (mTHPC) - chemical, pre-clinical and clinical developments in the last decade, *Photochem. Photobiol.* 99 (2023) 356–419, <https://doi.org/10.1111/php.13730>.
- [40] P. Franco, I. De Marco, The use of poly(N-vinyl pyrrolidone) in the delivery of drugs: a review, *Polymers (Basel)* 12 (2020) 1114, <https://doi.org/10.3390/polym12051114>.
- [41] Y.J. Eng, T.M. Nguyen, H.-K. Luo, J.M.W. Chan, Antifouling polymers for nanomedicine and surfaces: recent advances, *Nanoscale* 15 (2023) 15472–15512, <https://doi.org/10.1039/D3NR03164K>.
- [42] S. Ranjit, L. Malacrida, D.M. Jameson, E. Gratton, Fit-free analysis of fluorescence lifetime imaging data using the phasor approach, *Nat. Protoc.* 13 (2018) 1979–2004, <https://doi.org/10.1038/s41596-018-0026-5>.
- [43] N. Maldonado-Carmona, N. Villandier, T.-S. Ouk, Y. Launay, C.A. Calliste, A. Wiehe, S. Leroy-Lhez, Effect of the phenyl substituent's position on the encapsulation of porphyrins inside lignin nanoparticles: Photophysical and antibacterial properties, *J. Porphyrins Phthalocyanines* 26 (2022) 563–572, <https://doi.org/10.1142/s1088424622500237>.
- [44] I. Gjuroski, J. Furrer, M. Vermathen, How does the encapsulation of Porphyrinic photosensitizers into polymer matrices affect their self-association and dynamic properties? *ChemPhysChem* 19 (2018) 1089–1102, <https://doi.org/10.1002/cphc.201701318>.
- [45] T. Kellerer, J. Janusch, C. Freymüller, A. Rühm, R. Sroka, T. Hellerer, Comprehensive investigation of parameters influencing fluorescence lifetime imaging microscopy in frequency- and time-domain illustrated by phasor plot analysis, *Int. J. Mol. Sci.* 23 (2022) 15885, <https://doi.org/10.3390/ijms232415885>.
- [46] K. Hosomizu, M. Odoi, T. Umeyama, Y. Matano, K. Yoshida, S. Isoda, M. Isosomppi, N.V. Tkachenko, H. Lemmetyinen, H. Imahori, Substituent effects of Porphyrins on structures and Photophysical properties of amphiphilic porphyrin aggregates, *J. Phys. Chem. B* 112 (2008) 16517–16524, <https://doi.org/10.1021/jp807991k>.
- [47] M. Vermathen, M. Marzorati, P. Bigler, Self-assembling properties of Porphyrinic photosensitizers and their effect on membrane interactions probed by NMR spectroscopy, *J. Phys. Chem. B* 117 (2013) 6990–7001, <https://doi.org/10.1021/jp403331n>.
- [48] K. Kano, K. Fukuda, H. Wakami, R. Nishiyabu, R.F. Pasternack, Factors influencing self-aggregation tendencies of cationic porphyrins in aqueous solution, *J. Am. Chem. Soc.* 122 (2000) 7494–7502, <https://doi.org/10.1021/ja000738g>.
- [49] N.C. Maiti, S. Mazumdar, N. Periasamy, J- and H-aggregates of porphyrin-surfactant complexes: time-resolved fluorescence and other spectroscopic studies, *J. Phys. Chem. B* 102 (1998) 1528–1538, <https://doi.org/10.1021/jp972337z>.

- [50] F. Ricchelli, Photophysical properties of Porphyrins in biological-membranes, *J. Photochem. Photobiol. B Biol.* 29 (1995) 109–118, [https://doi.org/10.1016/1011-1344\(95\)07155-U](https://doi.org/10.1016/1011-1344(95)07155-U).
- [51] U. Rösch, S. Yao, R. Wortmann, F. Würthner, Fluorescent H-aggregates of Merocyanine dyes, *Angew. Chem. Int. Ed.* 45 (2006) 7026–7030, <https://doi.org/10.1002/anie.200602286>.
- [52] I.V. Tetko, J. Gasteiger, R. Todeschini, A. Mauri, D. Livingstone, P. Ertl, V. A. Palyulin, E.V. Radchenko, N.S. Zefirov, A.S. Makarenko, V.Y. Tanchuk, V. V. Prokopenko, Virtual computational chemistry laboratory - design and description, *J. Comput. Aided Mol. Des.* 19 (2005) 453–463, <https://doi.org/10.1007/s10822-005-8694-y>.
- [53] T.E. Zorina, I.V. Yankovsky, I.E. Kravchenko, T.V. Shman, M.V. Belevtsev, V. P. Zorin, Evaluation of Phototoxicity and cytotoxicity for chlorin e6 ester derivatives and their liposomal forms, *Biophysics* 60 (2015) 759–766, <https://doi.org/10.1134/S0006350915050267>.
- [54] L.M. Scolaro, M. Castriciano, A. Romeo, A. Mazzaglia, F. Mallamace, N. Micali, Nucleation effects in the aggregation of water-soluble porphyrin aqueous solutions, *Phys. A: Stat. Mech.* 304 (2002) 158–169, [https://doi.org/10.1016/S0378-4371\(01\)00547-7](https://doi.org/10.1016/S0378-4371(01)00547-7).
- [55] S. Paul, P.W.S. Heng, L.W. Chan, Optimization in solvent selection for Chlorin e6 in photodynamic therapy, *J. Fluoresc.* 23 (2013) 283–291.
- [56] M. Zannotti, R. Giovannetti, B. Minofar, D. Reha, L. Plačková, C.A. D'Amato, E. Rommozzi, H.V. Dudko, N. Kari, M. Minicucci, Aggregation and metal-complexation behaviour of THPP porphyrin in ethanol/water solutions as function of pH, *Spectrochim. Acta A Mol. Biomol. Spectrosc.* 193 (2018) 235–248, <https://doi.org/10.1016/j.saa.2017.12.021>.
- [57] R. Bonnett, B.D. Djelal, A. Nguyen, Physical and chemical studies related to the development of m-THPC (FOSCAN®) for the photodynamic therapy (PDT) of tumours, *J. Porphyrins Phthalocyanines* 05 (2001) 652–661, <https://doi.org/10.1002/jpp.377>.
- [58] Y. Guo, S. Huang, H. Sun, Z. Wang, Y. Shao, L. Li, Z. Li, F. Song, Tuning the aqueous self-assembly of porphyrins by varying the number of cationic side chains, *J. Mater. Chem. B* 10 (2022) 5968–5975, <https://doi.org/10.1039/D2TB00720G>.
- [59] T. Fukui, S. Kawai, S. Fujinuma, Y. Matsushita, T. Yasuda, T. Sakurai, S. Seki, M. Takeuchi, K. Sugiyasu, Control over differentiation of a metastable supramolecular assembly in one and two dimensions, *Nat. Chem.* 9 (2017) 493–499, <https://doi.org/10.1038/nchem.2684>.
- [60] M. Hädener, I. Gjurroski, J. Furrer, M. Vermathen, Interactions of Polyvinylpyrrolidone with Chlorin e6-based photosensitizers studied by NMR and electronic absorption spectroscopy, *J. Phys. Chem. B* 119 (2015) 12117–12128, <https://doi.org/10.1021/acs.jpcc.5b05761>.
- [61] S. Pfister, L. Sauser, I. Gjurroski, J. Furrer, M. Vermathen, Monitoring the encapsulation of chlorin e6 derivatives into polymer carriers by NMR spectroscopy, *J. Porphyrins Phthalocyanines* (2019), <https://doi.org/10.1142/S1088424619501815>.
- [62] S.M. Andrade, R. Teixeira, S.M. Costa, A.J. Sobral, Self-aggregation of free base porphyrins in aqueous solution and in DMPC vesicles, *Biophys. Chem.* 133 (2008) 1–10, <https://doi.org/10.1016/j.bpc.2007.11.007>.
- [63] P.S. Santiago, D.D. Neto, S.C.M. Gandini, M. Tabak, On the localization of water-soluble porphyrins in micellar systems evaluated by static and time-resolved frequency-domain fluorescence techniques, *Colloids Surf. B: Biointerfaces* 65 (2008) 247–256, <https://doi.org/10.1016/j.colsurfb.2008.04.010>.
- [64] M. Jadhao, P. Ahirkar, H. Kumar, R. Joshi, O.R. Meitei, S.K. Ghosh, Surfactant induced aggregation-disaggregation of photodynamic active chlorin e6 and its relevant interaction with DNA alkylating quinone in a biomimic micellar microenvironment, *RSC Adv.* 5 (2015) 81449–81460, <https://doi.org/10.1039/C5RA16181A>.
- [65] D.P. Ferreira, D.S. Conceição, R.C. Calhelha, T. Sousa, R. Socoteanu, I. Ferreira, L. F. Vieira Ferreira, Porphyrin dye into biopolymeric chitosan films for localized photodynamic therapy of cancer, *Carbohydr. Polym.* 151 (2016) 160–171, <https://doi.org/10.1016/j.carbpol.2016.05.060>.
- [66] S.C. Owen, D.P.Y. Chan, M.S. Shoichet, Polymeric micelle stability, *Nano Today* 7 (2012) 53–65, <https://doi.org/10.1016/j.nantod.2012.01.002>.
- [67] Ł. Lamch, R. Gancarz, M. Tsirigotis-Maniecka, I.M. Moszyńska, J. Ciejka, K.A. Wilk, Studying the “rigid-flexible” properties of polymeric micelle Core-forming segments with a hydrophobic Phthalocyanine probe using NMR and UV spectroscopy, *Langmuir* 37 (2021) 4316–4330, <https://doi.org/10.1021/acs.langmuir.1c00328>.
- [68] X. Liu, D. Lin, W. Becker, J. Niu, B. Yu, L. Liu, J. Qu, Fast fluorescence lifetime imaging techniques: a review on challenge and development, *J. Innov. Opt. Health Sci.* 12 (2019) 1930003, <https://doi.org/10.1142/s1793545819300039>.
- [69] G. Siboni, H. Weitman, D. Freeman, Y. Mazur, Z. Malik, B. Ehrenberg, The correlation between hydrophilicity of hypericins and helianthone: internalization mechanisms, subcellular distribution and photodynamic action in colon carcinoma cells, *Photochem. Photobiol. Sci.* 1 (2002) 483–491, <https://doi.org/10.1039/b202884k>.
- [70] A. Wiehe, E.J. Simonenko, M.O. Senge, B. Roder, Hydrophilicity vs hydrophobicity-varying the amphiphilic structure of porphyrins related to the photosensitizer m-THPC, *J. Porphyrins Phthalocyanines* 5 (2001) 758–761, <https://doi.org/10.1002/jpp.389>.
- [71] M. Marzorati, P. Bigler, M. Vermathen, Interactions between selected photosensitizers and model membranes: an NMR classification, *Biochim. Biophys. Acta Biomembr.* 2011 (1808) 1661–1672, <https://doi.org/10.1016/j.bbmem.2011.02.011>.
- [72] W. Jerjes, T.A. Theodossiou, H. Hirschberg, A. Høgsset, A. Weyergang, P.K. Selbo, Z. Hamdoun, C. Hopper, K. Berg, Photochemical internalization for intracellular drug delivery. From basic mechanisms to clinical research, *J. Clin. Med.* 9 (2020), <https://doi.org/10.3390/jcm9020528>.
- [73] M. Vermathen, M. Marzorati, P. Vermathen, P. Bigler, pH-dependent distribution of Chlorin e6 derivatives across phospholipid bilayers probed by NMR spectroscopy, *Langmuir* 26 (2010) 11085–11094, <https://doi.org/10.1021/la100679y>.
- [74] G. Parisio, M.M. Sperotto, A. Ferrarini, Flip-flop of steroids in phospholipid bilayers: effects of the chemical structure on Transbilayer diffusion, *J. Am. Chem. Soc.* 134 (2012) 12198–12208, <https://doi.org/10.1021/ja304007t>.
- [75] R. Bonnett, B.D. Djelal, P.A. Hamilton, G. Martínez, F. Wierrani, Photobleaching of 5,10,15,20-tetrakis(m-hydroxyphenyl)porphyrin (m-THPP) and the corresponding chlorin (m-THPC) and bacteriochlorin(m-THPBC). A comparative study, *J. Photochem. Photobiol. B Biol.* 53 (1999) 136–143, [https://doi.org/10.1016/S1011-1344\(99\)00139-6](https://doi.org/10.1016/S1011-1344(99)00139-6).
- [76] R. Bonnett, G. Martínez, Photobleaching of compounds of the 5,10,15,20-Tetrakis (m-hydroxyphenyl)porphyrin series (m-THPP, m-THPC, and m-THPBC), *Org. Lett.* 4 (2002) 2013–2016, <https://doi.org/10.1021/ol025842c>.
- [77] W. Peng, D.F. Samplonius, S. de Visscher, J.L. Roodenburg, W. Helfrich, M. J. Witjes, Photochemical internalization (PCI)-mediated enhancement of bleomycin cytotoxicity by liposomal mTHPC formulations in human head and neck cancer cells, *Lasers Surg. Med.* 46 (2014) 650–658, <https://doi.org/10.1002/lsm.22281>.
- [78] M. Millard, I. Yakavets, M. Piffoux, A. Brun, F. Gazeau, J.M. Guigner, J. Jasniowski, H.P. Lassalle, C. Wilhelm, L. Bezdtnaya, mTHPC-loaded extracellular vesicles outperform liposomal and free mTHPC formulations by an increased stability, drug delivery efficiency and cytotoxic effect in tridimensional model of tumors, *Drug Deliv.* 25 (2018) 1790–1801, <https://doi.org/10.1080/10717544.2018.1513609>.
- [79] M.O. Senge, J.C. Brandt, Temoporfin (Foscan®), 5,10,15,20-tetra(m-hydroxyphenyl)chlorin—a second-generation photosensitizer, *Photochem. Photobiol.* 87 (2011) 1240–1296, <https://doi.org/10.1111/j.1751-1097.2011.00986.x>.
- [80] D.J. Ball, D.I. Vernon, S.B. Brown, The high photoactivity of m-THPC in photodynamic therapy. Unusually strong retention of m-THPC by RIF-1 cells in culture, *Photochem. Photobiol.* 69 (1999) 360–363, [https://doi.org/10.1562/0031-8655\(1999\)069<0360:thpvt>2.3.co;2](https://doi.org/10.1562/0031-8655(1999)069<0360:thpvt>2.3.co;2).
- [81] A.L. Luss, P.P. Kulikov, S.B. Romme, C.L. Andersen, C.P. Pennisi, A.O. Docea, A. N. Kuskov, K. Velonia, Y.O. Mezhuev, M.I. Shtilman, A.M. Tsatsakis, L. Gurevich, Nanosized carriers based on amphiphilic poly-N-vinyl-2-pyrrolidone for intranuclear drug delivery, *Nanomedicine (London)* 13 (2018) 703–715, <https://doi.org/10.2217/nmm-2017-0311>.
- [82] M. Demazeau, L. Gibot, A.-F. Mingotaud, P. Vicendo, C. Roux, B. Lonetti, Rational design of block copolymer self-assemblies in photodynamic therapy, *Beilstein J. Nanotechnol.* 11 (2020) 180–212, <https://doi.org/10.3762/bjnano.11.15>.
- [83] U. Till, L. Gibot, A.-F. Mingotaud, J. Ehrhart, L. Wasungu, C. Mingotaud, J.-P. Souchard, A. Poinso, M.-P. Rols, F. Violleau, P. Vicendo, Drug release by direct jump from poly(ethylene-glycol-b-ε-caprolactone) Nano-vector to cell membrane, *Molecules* 21 (2016) 1643, <https://doi.org/10.3390/molecules21121643>.
- [84] G. Sahay, E.V. Batrakova, A.V. Kabanov, Different internalization pathways of polymeric micelles and unimers and their effects on vesicular transport, *Bioconjug. Chem.* 19 (2008) 2023–2029, <https://doi.org/10.1021/bc8002315>.
- [85] M.H. Teiten, L. Bezdtnaya, P. Morlière, R. Santus, F. Guillemain, Endoplasmic reticulum and Golgi apparatus are the preferential sites of Foscan® localisation in cultured tumour cells, *Br. J. Cancer* 88 (2003) 146–152, <https://doi.org/10.1038/sj.bjc.6600664>.